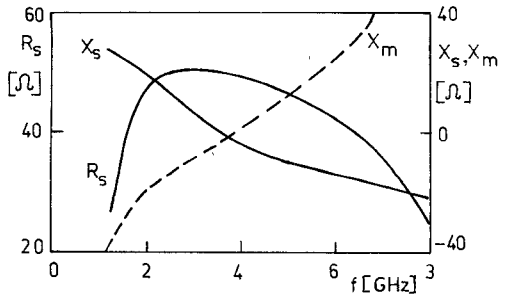

Fig. 8. Frequency characteristics of R_s, X_s, X_m. $l_r = 6.5$ mm, $w_r = 7.5$ mm.

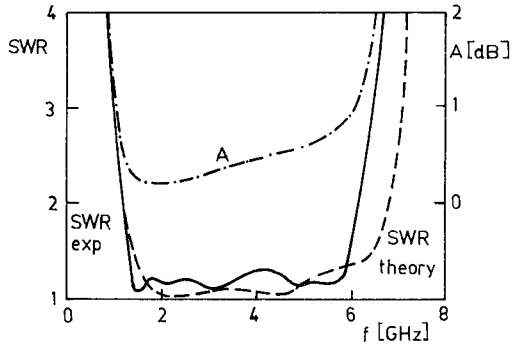

Fig. 9. Theoretical SWR characteristics of single microstrip–slotline transition and experimental characteristics of two cascade-connected transitions. A: insertion loss. $h = 1.5$ mm, $\epsilon_r = 9.8$.

below 1.45 in the frequency range 2 to 12.7 GHz with a local increase to 1.6 in the vicinity of 8 GHz. The achieved bandwidth is comparable to that reported by Schüppert [6] for a similar transition. The midband performance of the realized transitions is, however, somewhat better, which is attributed to the inclusion of the slotline–microstrip voltage transformation ratio n in the modeling.

V. Conclusions

A resonant technique has been described that allows the accurate measurement of slotline short- and open-circuit equivalent reactances. Numerous experimental results have been given for circuits on an alumina substrate ($\epsilon = 9.8$). These include a graph of planar short-end reactance for normalized slot width values of 0.05 to 2 as well as the frequency characteristics of several open circuits. It has been demonstrated that these open circuits behave as nonuniform resonators with the resulting bandwidth limitation. A 1.5–6 GHz low SWR microstrip–slotline transition design has been presented that employs one of the measured open circuits. A 2–12.7 GHz transition has been obtained by scaling the first transition to a thinner substrate.

References

[1] J. B. Knorr and J. Saenz, "End effect in shorted slot," *IEEE Trans. Microwave Theory Tech.*, vol. MTT-21, pp. 579–580, 1973.

[2] B. Easter, J. G. Richings, and I. M. Stephenson, "Resonant techniques for the accurate measurement of microstrip properties and equivalent circuits," in *Proc. 3rd European Microwave Conf.*, 1973, paper B. 7.5.

[3] E. Pic and W. J. R. Hoefer, "Experimental characterization of finline discontinuities using resonant techniques," in *IEEE MTT-S Int. Microwave Symp. Dig.*, 1981, pp. 108–110

[4] J. Q. Howell, "A quick, accurate method to measure the dielectric constant of MIC substrates," *IEEE Trans. Microwave Theory Tech.*, vol. MTT-21, pp. 142–143, 1973.

[5] K. C. Gupta, R. Garg and I. J. Bahl, *Microstrip Lines and Slotlines*. Dedham, MA: Artech House, 1979.

[6] B. Schüppert, "Microstrip–slotline transitions: Modeling and experimental investigation," *IEEE Trans. Microwave Theory Tech.*, vol. 36, pp. 1272–1282, 1988.

[7] A. Podcameni and M. L. Coimbra, "Slotline–microstrip transition on iso/anisotropic substrate: A more accurate design," *Electron. Lett.*, vol. 16, pp. 780–781, 1980.

A Moment Method Solution of a Volume–Surface Integral Equation Using Isoparametric Elements and Point Matching

JIAN-MING JIN, STUDENT MEMBER, IEEE, JOHN L. VOLAKIS, SENIOR MEMBER, IEEE, AND VALDIS V. LIEPA, MEMBER, IEEE

***Abstract*—It is shown that traditional subdomain elements such as rectangles and triangles with a pulse expansion basis could lead to inaccuracies when simulating biological scatterers having high permittivities. In this paper, isoparametric elements are used in a moment method implementation to remove modeling inaccuracies of fields and boundaries associated with traditional elements. Numerical results are also given that show the improvement achieved in the scattering solution for high-contrast circular cylinders.**

I. Introduction

A volume–surface integral equation (VSIE) was recently presented [1], [2] for electromagnetic scattering by inhomogeneous cylinders. A moment method (MM) solution of the VSIE was also considered using rectangular and triangular elements with pulse expansion basis functions and point matching. Such a moment method solution, however, becomes inaccurate in the case of scatterers having high permittivities with transverse electric (TE) incidence or high permeabilities with transverse magnetic (TM) incidence. To overcome this difficulty, in this paper we develop a MM solution by employing isoparametric elements.

Isoparametric elements were first introduced in finite element analysis [3]. The main advantage of using such elements is to allow an accurate modeling of arbitrarily shaped geometries. However, it appears that only recently [4] have they been employed in solutions of volume integral equations for electromagnetics. Below we first discuss the inaccuracy associated with traditional solutions of integral equations for penetrable scatterers having high refractive indices. This is followed by the introduction of isoparametric elements and the presentation of the MM solution of the VSIE using such elements. Results are subsequently presented which show the stability of the solution in the case of cylindrical geometries associated with high refractive indices.

II. Discussion of the Integral Equations

In this section we first examine the VSIE for the computation of the internal fields in a cylinder having nonunity relative permittivity ϵ_r and permeability μ_r. Assuming the cylinder has its

Manuscript received November 28, 1988; revised May 4, 1989 This work was supported in part by the NASA Ames Research Center under Grant NAG-2-541.

The authors are with the Radiation Laboratory, Department of Electrical Engineering and Computer Science, University of Michigan, Ann Arbor, MI 48109.

IEEE Log Number 8929926.

infinite dimension along the z axis, we have that the field satisfies the general VSIE [1]:

$$F^{\mathrm{INC}}(\boldsymbol{r}) + k_0^2 \int\int_{\Omega} [v(\boldsymbol{r}') - u(\boldsymbol{r}')] F(\boldsymbol{r}') G_0(\boldsymbol{r}|\boldsymbol{r}')\, ds' + \int\int_{\Omega} \nabla' u(\boldsymbol{r}') \cdot [F(\boldsymbol{r}') \nabla' G_0(\boldsymbol{r}|\boldsymbol{r}')]\, ds' + \oint_{\Gamma} [u(\boldsymbol{r}'_+) - u(\boldsymbol{r}'_-)] F(\boldsymbol{r}') \frac{\partial G_0(\boldsymbol{r}|\boldsymbol{r}')}{\partial n'}\, dl' = \begin{cases} u(\boldsymbol{r}) F(\boldsymbol{r}) & \text{for } \boldsymbol{r} \text{ not on } \Gamma \\ \frac{1}{2}[u(\boldsymbol{r}_+) + u(\boldsymbol{r}_-)] F(\boldsymbol{r}) & \text{for } \boldsymbol{r} \text{ on } \Gamma \end{cases} \quad (1)$$

where

$$F(\boldsymbol{r}) = E_z(\boldsymbol{r}) \qquad u(\boldsymbol{r}) = \frac{1}{\mu_r(\boldsymbol{r})} \qquad v(\boldsymbol{r}) = \epsilon_r(\boldsymbol{r})$$

for TM incidence and

$$F(\boldsymbol{r}) = H_z(\boldsymbol{r}) \qquad u(\boldsymbol{r}) = \frac{1}{\epsilon_r(\boldsymbol{r})} \qquad v(\boldsymbol{r}) = \mu_r(\boldsymbol{r})$$

for TE incidence, in which E_z and H_z denote the z components of the electric and magnetic fields, respectively, F^{INC} denotes the corresponding incident field, and $G_0(\boldsymbol{r}|\boldsymbol{r}')$ is the two-dimensional free-space Green's function. In addition, Ω denotes the region occupied by the cylinder, Γ denotes the interface where $u(\boldsymbol{r})$ has a step discontinuity, $\hat{n}$ is the unit vector normal to Γ pointing from the "$-$" side to the "$+$" side and $\oint$ denotes the Cauchy principal value integral.

Let us now examine the numerical implications which may arise when the VSIE is implemented in the case of large $|\epsilon_r|$ with TE incidence. We observe that the right-hand side of (1) is proportional to $1/|\epsilon_r|$ for nominal values of the internal field H_z. For large $|\epsilon_r|$ this implies that the integrals over Ω and Γ must together give a value nearly equal to the negative of H_z^{INC}. That is, if $|\epsilon_r| = 100$ and we demand a 1 percent solution accuracy for the internal fields, the integrals must be computed with a corresponding accuracy of 0.01 percent. In general, the presence of $|\epsilon_r|$ acts as an error amplifier and we may conclude that, for a solution accuracy of δ percent, the integrals must be evaluated with a corresponding accuracy of $\delta/|\epsilon_r|$ percent. This statement has been experimentally verified and, clearly, for large $|\epsilon_r|$ a crude discretization is unlikely to produce the accuracy demanded here. The same conclusion holds for the case of large $|\mu_r|$ with TM incidence.

A similar examination of the electric field integral equation (EFIE) given by Borup *et al.* [5, eq. (1)] for TE scattering also reveals that for a desired solution accuracy of δ percent, the integrals in the EFIE must be evaluated with a corresponding accuracy of δ/m percent, where $m = |\boldsymbol{E}_t^{\mathrm{INC}}|/|\boldsymbol{E}_t| \approx \sqrt{\epsilon_r}$. Thus, even though the EFIE is slightly less demanding in accuracy, it is still unstable for scatterers with large refractive indices. This exposition satisfactorily explains the difficulties encountered in [5] as well as the success of their modified approach. Also, the results given by Boyes and Kennedy [6] can be explained in this manner.

When we examine the magnetic field integral equation (MFIE) presented by Peterson and Klock [7, eq. (2)] for TE scattering, we find that the MFIE is more stable than the VSIE and EFIE; however, it involves a second derivative of the unknown field quantity and as a result demands higher order basis functions. In particular, the VSIE can be implemented with a pulse basis and the EFIE with a linear basis but the MFIE requires a quadratic basis.[1] Since the introduction of a quadratic basis in the VSIE and EFIE will improve their accuracy, there is no clear choice in deciding which of the three is more attractive for numerical implementation. Each is certainly associated with its own advantages and disadvantages for large refractive indices, but for nominal values of ϵ_r the VSIE given in (1) is generally superior over the others.

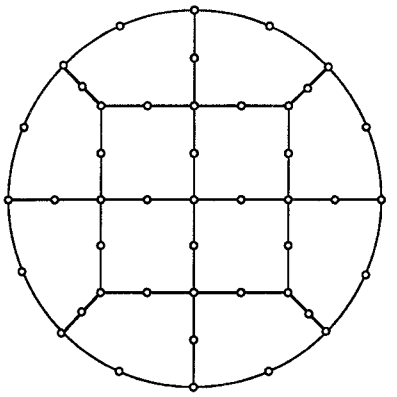

Fig. 1. An example for breaking a circular region: a 12 quadrilateral element model with 45 nodes.

In the next section we consider an implementation of the VSIE using isoparametric elements which can provide accurate geometrical simulation and field representation. They are, therefore, expected to provide the required accuracy for the simulation of high-contrast dielectrics.

III. Formulation with Isoparametric Elements and Point Matching

In this section we describe a numerical solution of the VSIE using isoparametric elements with point matching. For convenience, we can write (1) as

$$F^{\mathrm{INC}}(\boldsymbol{r}) + \int\int_{\Omega} A(\boldsymbol{r}|\boldsymbol{r}')\, F(\boldsymbol{r}')\, ds' + \oint_{\Gamma} B(\boldsymbol{r}|\boldsymbol{r}')\, F(\boldsymbol{r}')\, dl' = \begin{cases} u(\boldsymbol{r}) F(\boldsymbol{r}) & \text{for } \boldsymbol{r} \text{ not on } \Gamma \\ \frac{1}{2}[u(\boldsymbol{r}_+) + u(\boldsymbol{r}_-)] F(\boldsymbol{r}) & \text{for } \boldsymbol{r} \text{ on } \Gamma \end{cases} \quad (2)$$

where the expressions for $A(\boldsymbol{r}|\boldsymbol{r}')$ and $B(\boldsymbol{r}|\boldsymbol{r}')$ are determined by direct comparison with (1).

In a numerical solution of (1) or (2) using isoparametric elements, the two-dimensional region Ω is broken up into a number of quadrilaterals whose sides can be curved, as shown, for example, in Fig. 1. A usual rule for this subdivision is that the interface Γ coincides with the boundaries of the quadrilaterals. Assuming now that the discretization results in $M2$ quadrilaterals and that $M1$ curved segments make up the contour(s) Γ, (2)

[1] If ϵ_r is uniform within each element, the corresponding basis functions can be one order lower.

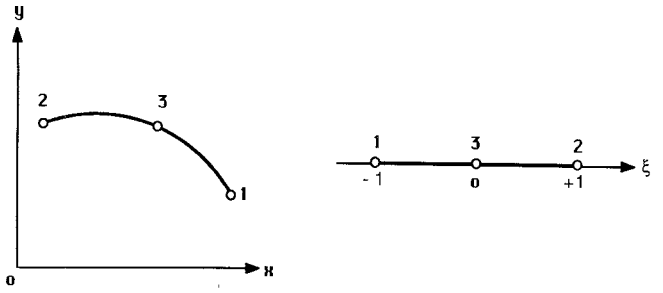

Fig. 2. A quadratically curved segment in the xy plane can be transformed into a straight segment lying on the ϵ axis.

becomes

$$F^{\mathrm{INC}}(\boldsymbol{r}) + \sum_{e=1}^{M2}\sum_{i=1}^{n2} \phi_i^e \int\int_{\Omega^e} A(\boldsymbol{r}|\boldsymbol{r}')\, V_i^e(\boldsymbol{r}')\, ds' + \sum_{s=1}^{M1}\sum_{i=1}^{n1} \phi_i^s \oint_{\Gamma^s} B(\boldsymbol{r}|\boldsymbol{r}')\, U_i^s(\boldsymbol{r}')\, dl' = \begin{cases} u(\boldsymbol{r})\, F(\boldsymbol{r}) & \text{for } \boldsymbol{r} \text{ not on } \Gamma \\ \dfrac{1}{2}\left[u(\boldsymbol{r}_+) + u(\boldsymbol{r}_-)\right] F(\boldsymbol{r}) & \text{for } \boldsymbol{r} \text{ on } \Gamma. \end{cases} \tag{3}$$

In (3), the field in the eth quadrilateral has been expanded as

$$F^e(\boldsymbol{r}) = \sum_{i=1}^{n2} V_i^e(\boldsymbol{r})\, \phi_i^e \tag{4}$$

where $V_i^e(\boldsymbol{r})$ $(i=1,2,\cdots,n2)$ are a set of known expansion basis functions and ϕ_i^e $(i=1,2,\cdots,n2)$ are the corresponding unknown coefficients. Similarly, the field in the sth segment was expanded as

$$F^s(\boldsymbol{r}) = \sum_{i=1}^{n1} U_i^s(\boldsymbol{r})\, \phi_i^s \tag{5}$$

where $U_i^s(\boldsymbol{r})$ $(i=1,2,\cdots,n1)$ represent the known expansion basis functions and ϕ_i^s $(i=1,2,\cdots,n1)$ are the unknown constants.

Before proceeding with a solution of (3) it is first necessary to choose the basis functions $V_i^e(\boldsymbol{r})$ and $U_i^s(\boldsymbol{r})$ in accordance with the definition of the isoparametric elements. A possible method of constructing U_i^s and V_i^e is to choose them so that ϕ_i^s $(i=1,2,\cdots,n1)$ represent the field values at $n1$ nodes on the sth segment and likewise ϕ_i^e $(i=1,2,\cdots,n2)$ represent the field values at $n2$ nodes of the eth quadrilateral. A point-matching procedure applied to (3) will then lead to a matrix equation for the solution of the nodal field values.

To find U_i^s as described above it is convenient to introduce the transformation

$$x = \sum_{i=1}^{3} L_i^s(\xi)\, x_i \qquad y = \sum_{i=1}^{3} L_i^s(\xi)\, y_i \tag{6}$$

allowing a linearization of a quadratically curved segment as shown in Fig. 2. In (6), L_i^s $(i=1,2,3)$ are the shape functions which take the well-known form [3]

$$L_1^s = -\frac{1}{2}(1-\xi)\xi \qquad L_2^s = \frac{1}{2}(1+\xi)\xi \qquad L_3^s = 1-\xi^2.$$

In addition, (6) implies the relation

$$dl = \sqrt{\left(\frac{\partial x}{\partial \xi}\right)^2 + \left(\frac{\partial y}{\partial \xi}\right)^2}\, d\xi = |J^s|\, d\xi \tag{7}$$

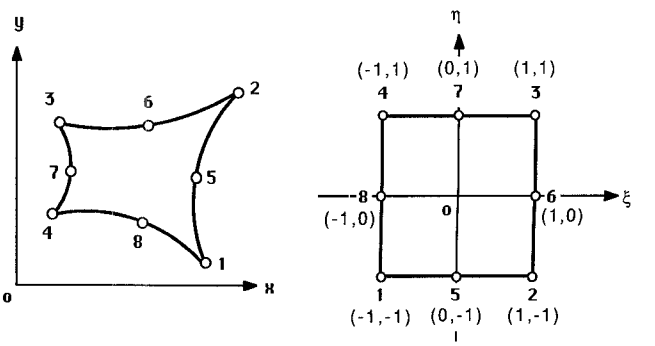

Fig. 3. A quadrilateral element with quadratically curved sides in the xy plane can be transformed into a square in the local $\xi\eta$ plane.

and the unit vector $\hat{n}$ is now given by

$$\hat{n} = \left(\hat{x}\frac{\partial y}{\partial \xi} - \hat{y}\frac{\partial x}{\partial \xi}\right)|J^s|^{-1}. \tag{8}$$

It is observed that $L_i^s(\xi)$ is unity at the ith node and thus by choosing $U_i^s = L_i^s$, ϕ_i^s will coincide with the nodal values of the field $F^s(\boldsymbol{r})$. This is actually the definition of the isoparametric elements since L_i^s describe the geometrical shape of the discrete elements. When this expansion is substituted in (3), it leads to integrals of the form

$$I^s = \int_{\Gamma^s} B(\boldsymbol{r}|\boldsymbol{r}')\, L_i^s(\xi')\, dl' = \int_{-1}^{1} B(\boldsymbol{r}|\boldsymbol{r}')\, L_i^s(\xi')\, |J^s(\xi')|\, d\xi' \tag{9}$$

and these can be evaluated via a four-point Gaussian integration formula giving

$$I^s = \sum_{j=1}^{4} W_j B(\boldsymbol{r}|\boldsymbol{r}_j')\, L_i^s(\xi_j)\, |J^s(\xi_j)| \tag{10}$$

where $\xi_1 = -\xi_4 = -0.8611363116$, $\xi_2 = -\xi_3 = -0.3399810436$, $W_1 = W_4 = 0.3478548451$, $W_2 = W_3 = 0.6521451549$, and $\boldsymbol{r}_j' = x(\xi_j)\hat{x} + y(\xi_j)\hat{y}$, in which $x(\xi_j)$ and $y(\xi_j)$ are given by (6).

The treatment of the area integral over Ω follows a similar procedure. We can again introduce the transformation

$$x = \sum_{i=1}^{8} N_i^e(\xi,\eta)\, x_i \qquad y = \sum_{i=1}^{8} N_i^e(\xi,\eta)\, y_i \tag{11}$$

allowing the representation of an arbitrarily shaped quadrilateral with quadratically curved sides in the xy plane to a square in the $\xi\eta$ plane as shown in Fig. 3. The shape functions are now N_i^e $(i=1,2,\cdots,8)$ and they take the known form [3]

$$N_1^e = -\frac{1}{4}(1-\xi)(1-\eta)(\xi+\eta+1)$$

$$N_2^e = \frac{1}{4}(1+\xi)(1-\eta)(\xi-\eta-1)$$

$$N_3^e = \frac{1}{4}(1+\xi)(1+\eta)(\xi+\eta-1)$$

$$N_4^e = \frac{1}{4}(1-\xi)(1+\eta)(-\xi+\eta-1)$$

$$N_5^e = \frac{1}{2}(1-\xi^2)(1-\eta) \qquad N_6^e = \frac{1}{2}(1+\xi)(1-\eta^2)$$

$$N_7^e = \frac{1}{2}(1-\xi^2)(1+\eta) \qquad N_8^e = \frac{1}{2}(1-\xi)(1-\eta^2).$$

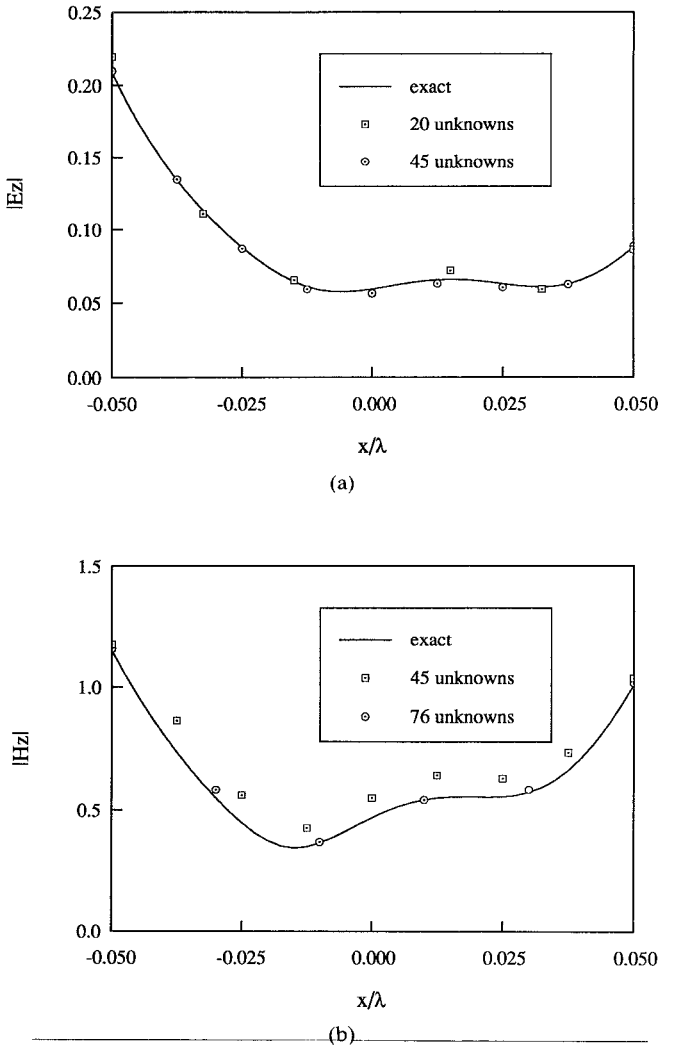

Fig. 4. The axial field along the x axis inside a homogeneous dielectric circular cylinder of radius $a = 0.05\lambda$ and $\epsilon_r = 72.0 - j162.0$. (a) TM incidence; (b) TE incidence.

With this transformation the area element ds can be expressed as

$$ds = |J^e|\, d\xi\, d\eta \tag{12}$$

in which

$$|J^e| = \frac{\partial x}{\partial \xi}\frac{\partial y}{\partial \eta} - \frac{\partial x}{\partial \eta}\frac{\partial y}{\partial \xi}$$

is the determinant of the Jacobian transformation matrix. As in the one-dimensional case, the shape function $N_i^e(\xi, \eta)$ is unity when $\xi = \xi_i$ and $\eta = \eta_i$. Thus, in accordance with the definition of the isoparametric elements, we choose $V_i^e = N_i^e$ and as such the coefficients ϕ_i^e will coincide with the nodal values of the field $F^e(\boldsymbol{r})$. When this expansion is substituted in (3) we obtain integrals of the form

$$I^e = \int\int_{\Omega^e} A(\boldsymbol{r}|\boldsymbol{r}')\, N_i^e(\boldsymbol{r}')\, ds'$$

$$= \int_{-1}^{1}\int_{-1}^{1} A(\boldsymbol{r}|\boldsymbol{r}')\, N_i^e(\xi', \eta')\, |J^e(\xi', \eta')|\, d\xi' d\eta' \tag{13}$$

and by using a nine-point Gaussian integration formula, I^e can be written as

$$I^e = \sum_{j=1}^{3}\sum_{k=1}^{3} W_j W_k A(\boldsymbol{r}|\boldsymbol{r}'_{jk})\, N_i^e(\xi_j, \eta_k)\, |J^e(\xi_j, \eta_k)| \tag{14}$$

where $\xi_1 = \eta_1 = -\xi_3 = -\eta_3 = -0.7745966692$, $\xi_2 = \eta_2 = 0.0$, $W_1 = W_3 = 0.5555555556$, $W_2 = 0.8888888889$, and $\boldsymbol{r}'_{jk} = x(\xi_j, \eta_k)\hat{x} + y(\xi_j, \eta_k)\hat{y}$, with $x(\xi_j, \eta_k)$ and $y(\xi_j, \eta_k)$ as given in (11).

The numerical implementation of the above formulation is rather straightforward. However, the accuracy of the solution will be seen to be remarkable for scatterers having large values of u.

TABLE I
BISTATIC RADAR CROSS SECTION (σ/λ) FOR A HOMOGENEOUS DIELECTRIC CIRCULAR CYLINDER WITH RADIUS $a = 0.05\lambda$ AND $\epsilon_r = 72.0 - j162.0$

	TM case			TE case		
Angle (deg.)	20 unk	45 unk	Exact	45 unk	76 unk	Exact
0	-4 03	-3.96	-3 95	-20.44	-20.46	-20.54
60	-4.63	-4 56	-4.55	-30.28	-28.93	-28.99
120	-5.89	-5.83	-5.82	-19.99	-19 72	-19.65
180	-6.56	-6 49	-6.49	-15.85	-15.75	-15 71

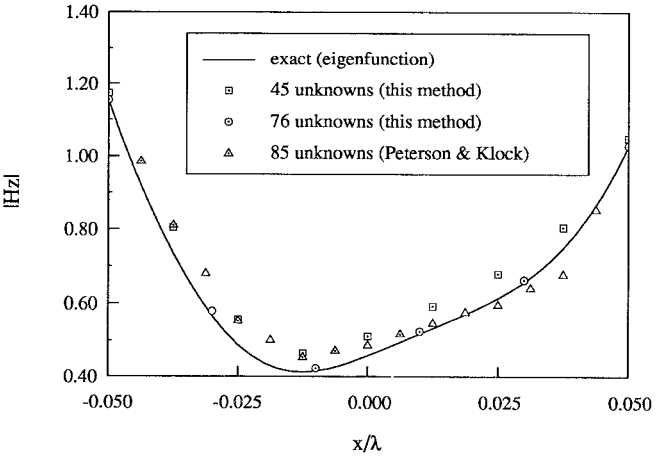

Fig. 5 The magnetic field along the x axis inside a homogeneous dielectric circular cylinder of radius $a = 0\ 05\lambda$ and $\epsilon_r = 4\ 0 - j100.0$ for TE incidence. A comparison with exact data and those given in [7].

IV. NUMERICAL RESULTS

To validate the above MM formulation and show its usefulness, we performed a few numerical experiments. For the results shown below, the incident field is assumed to be a plane wave propagating in the x direction and the axis of the cylinder is coincident with the z axis.

We first consider a dielectric circular cylinder with a radius 0.05λ (free space wavelength) and relative permittivity as high as $\epsilon_r = 72.0 - j162.0$, corresponding to a muscle cylinder at 100 MHz. Fig. 4 shows the electric and magnetic fields inside the cylinder for the TM and TE cases, respectively. Also, Table I gives the bistatic radar cross section, all compared with the exact eigenfunction solutions. As seen, there is an excellent agreement when the element size is chosen sufficiently small. We note that our previous MM codes [1], [2] employing rectangular and triangular elements with pulse basis functions are unable to predict the correct TE result shown in Fig. 4(b). A similar conclusion was also reached by Peterson and Klock [7] when they examined

Richmond's [8] formulation, where pulse basis functions were employed for the solution of the electric field integral equation.

In [7], Peterson and Klock presented a solution of an improved magnetic field integral equation by employing triangular elements with linear basis functions in the TE case. Here we compare our results with those in [7] for a dielectric cylinder with a radius 0.05λ having a relative permittivity $\epsilon_r = 4.0 - j100.0$. The results are shown in Fig. 5 and, as seen, the present approach provides a higher accuracy.

V. Conclusion

In this paper, we examined three integral equations for TE scattering by dielectric cylinders having large values of permittivity. A moment method solution of the volume–surface integral equation was then developed by employing isoparametric elements and point matching. Differing from the traditional solutions using pulse basis, the one presented here was shown to be more accurate and stable, particularly in the case of scatterers having large refractive indices.

References

[1] J. M Jin, V. V. Liepa, and C. T Tai, "A volume-surface integral equation for electromagnetic scattering by inhomogeneous cylinders," *J. Electromagnetic Waves and Applications*, vol. 2, pp. 573–588, 1988.

[2] M. A. Ricoy, S. Kilberg, and J. L. Volakis, "A simple set of integral equations for two-dimensional scattering with further reduction on unknowns," *Proc. Inst. Elec. Eng*, pt. H, 1989.

[3] O. C. Zienkiewicz, *The Finite Element Method*, 3rd ed. New York: McGraw-Hill, 1977

[4] R. D Graglia, "The use of parametric elements in the moment method solution of static and dynamic volume integral equations," *IEEE Trans. Antennas Propagat.*, vol. 36, pp. 636–646, 1988.

[5] D. T Borup, D. M. Sullivan, and O. P. Gandhi, "Comparison of the FFT conjugate gradient method and the finite-difference time-domain method for the 2-D absorption problem," *IEEE Trans. Microwave Theory Tech.*, vol. MTT-35, pp. 383–395, 1987.

[6] W. E. Boyse and W D Kennedy, "A study of two-dimensional cylinders illuminated by TE polarized microwaves using the k-space algorithm," in *1988 IEEE AP-S Int Symp. Dig.* (Syracuse, NY), June 1988, pp. 84–87.

[7] A. F. Peterson and P. W Klock, "An improved MFIE formulation for TE-scattering from lossy, inhomogeneous dielectric cylinders," *IEEE Trans. Antennas Propagat.*, vol. 36, pp. 45–49, 1988.

[8] J. H. Richmond, "TE-wave scattering by a dielectric cylinder of arbitrary cross-section shape," *IEEE Trans. Antennas Propagat.*, vol. AP-14, pp. 460–464, 1966

Characteristic Impedance of a Tubular Dielectric Cylinder Covered with Conducting Arc Strips

V. ZARGARI AND T. C. RAO, SENIOR MEMBER, IEEE

Abstract—**The characteristic impedance of a circular cylindrical dielectric tubular transmission line that is partially covered by thin conducting arc strips on the outer periphery is determined by conformal transformation. The variation of the characteristic impedance with the physical parameters is studied and some numerical results are presented.**

I. Introduction

Circular cylindrical dielectric waveguides that are partially covered with infinitesimally thin conducting coatings on the outer periphery have many potential applications in the design of transitions, baluns, and impedance transformers. Cylindrical stripline and cylindrical microstrip line fall into this category. Assuming that only the TEM mode exists, Wang [1] solved Laplace's equation by a dual series method and presented extensive results on the characteristic impedance of such lines. Joshi and Das [2] analyzed the problem of a cylindrical stripline with a homogeneous dielectric medium by a conformal transformation technique. Later, Joshi *et al.* [3] used the logarithmic transformation and reduced the problem of cylindrical stripline to an equivalent planar geometry. Recently, Zeng and Wang [4] also used conformal transformation to find expressions for the characteristic impedance in a closed form for cylindrical and elliptical striplines and microstrip lines with zero and finite-thickness strip conductors. Reddy and Deshpande [5] obtained a closed-form expression for the characteristic impedance of a cylindrical stripline with multilayer dielectrics.

In the present article, the transmission line consists of a hollow dielectric tube with two infinitely long thin conducting arc strips on the outer periphery, as shown in Fig. 1(a). Alternatively, the line can also take the complementary form shown in Fig. 1(b). The characteristic impedance is determined by first transforming the geometry to an equivalent planar geometry. In the planar form, the structure shown in Fig. 1(a) is similar to the coplanar stripline (CPS), while the geometry of Fig. 1(b) is similar to the coplanar waveguide (CPW) originally proposed by Wen [6]. The characteristic impedance of these lines can easily be found from the design equations given by Gupta *et al.* [7].

II. Theory

A hollow dielectric tube of permittivity ϵ_r, internal radius a, and external radius b is considered whose transverse cross section is shown in Fig. 1(a). Two infinitesimally thin conducting arc strips of width $b\phi$, symmetrically located with respect to the y axis, are located on the outer boundary of the dielectric. The geometry shown in Fig. 1(b) is complementary to that of Fig. 1(a), where the positions of slot and the arc strips are interchanged. The angular separation between the strips (or slots) is denoted by 2ψ. The two geometries of Fig. 1 can be transformed into planar geometries with the transformation function

$$w = \pi/2 + j \ln z \tag{1a}$$

where

$$z = x + jy \qquad w = u + jv \tag{1b}$$

refer to the variables in the original geometry and the transformed geometry, as shown in Fig. 2. The surfaces $\rho = a$ and $\rho = b$ transform to the straight lines v_1 and v_2, given by

$$v_1 = \ln a \tag{2}$$

$$v_2 = \ln b. \tag{3}$$

The distance between the two planes v_1 and v_2 becomes

$$h = \ln(b/a). \tag{4}$$

The width of the conducting strips (or slots) becomes

$$w_1 = \phi \tag{5}$$

and the spacing between them becomes

$$S = 2\psi. \tag{6}$$

The characteristic impedance of a coplanar waveguide (CPW) was calculated by Wen [6] by a quasi-static analysis and conformal mapping, where the dielectric substrate thickness was assumed to be sufficiently large to be considered infinite. For

Manuscript received December 12, 1988; revised April 26, 1989.

The authors are with the Microwave Laboratory, Department of Electrical Engineering, University of Lowell, Lowell, MA 01854.

IEEE Log Number 8929927.

0018-9480/89/1000-1645$01.00 ©1989 IEEE